Vertical arrays of nanofluidic channels fabricated without nanolithography†

Roman Sordan,*[a] Alessio Miranda,[a] Floriano Traversi,[a] Davide Colombo,[a] Daniel Chrastina,[a] Giovanni Isella,[a] Massimo Masserini,[b] Leo Miglio,[c] Klaus Kern[de] and Kannan Balasubramanian[d]

Received 3rd November 2008, Accepted 4th February 2009
First published as an Advance Article on the web 3rd March 2009
DOI: 10.1039/b819520j

Vertical arrays of sealed nanofluidic channels, in which both cross-sectional dimensions are controllable down to 10 nm, were fabricated by selective side etching of a SiGe heterostructure comprised of layers of alternating Ge fractions. Capillary filling of these nanochannel arrays with fluorescent dye solutions was investigated using a confocal microscope. The feasibility of using nanochannels for size-based separation of biomolecules was demonstrated by imaging aggregates of tagged amyloid-beta peptide. The ability to integrate a large number of nanochannels shows promise for high throughput applications involving lab-on-a-chip systems.

Introduction

Biochemical reactions usually involve a large number of protein and nucleic acid molecules interacting at the nanoscale level. Exploring the microscopic basis of such reactions is often obscured because averaged responses from an enormous number of individual molecules are measured in the experiment. The ability to separate, isolate, and investigate a small number of molecules in a nanoscale-confined environment is a long-sought after goal of molecular diagnostics. With recent advances in nanoscience and nanotechnology, this goal has been brought closer to reality by the use of nanoscale channels[1,2] for fluid flow in place of microfluidic channels.[3,4] Nanofluidic systems enable the study of physical principles[5,6] and biomolecular interactions in a controllable fluidic environment at a scale that has not yet been directly accessible. From an application point of view, lab-on-a-chip devices based on nanofluidic channels show promise for achieving absolute single molecule sensitivity combined with high selectivity along with the advantages of high throughput, low access times, and extremely small sample volumes (pL to fL range).

The affordability of a molecular diagnostic platform is commonly at odds with the nanoscale requirements of single-biomolecular studies. To overcome this constraint, alternative technologies have recently been developed in order to fabricate nanofluidic channels without expensive (in terms of cost per chip) top-down nanolithography. A spacer patterning technique[7] is a common choice if nanochannels are to be fabricated in a standard Si technology. This method has been implemented by etching material deposited,[8] oxidized,[9] or unoxidized[10] on the sidewall of a step, or by fabricating a nanoimprint mold used to imprint nanochannels.[11,12] Side etching[13] of a patterned[8] or unpatterned[14] thin sacrificial layer has also been used to form nanochannels within the step sidewall. However, these technologies lack the ability to integrate nanofluidic channels in a vertical arrangement (similar to layers in integrated circuits) without significant increases in fabrication complexity. Three dimensional (3D) stacks of nanochannels would provide a fundamental improvement over current planar technologies by significantly increasing the density of nanochannels, enabling large scale integration, parallel processing, portability, and high sensitivity.[15–17] Here we demonstrate a simple conventional process technology capable of producing 3D arrays of nanofluidic channels with nanoscale ($\sim$10 nm) cross-sectional dimensions. The nanochannels were fabricated by selective side etching of multiple epitaxially-grown sacrificial layers and were subsequently sealed by deposition of material by evaporation. The present fabrication process is compatible with standard semiconductor technology enabling simple integration with conventional electronic and fluidic devices for fast on-chip processing. The suitability of the fabricated nanochannels for nanofluidic applications is demonstrated by observing the flow of a fluorescent dye solution through the nanochannels with the help of a confocal laser scanning microscope. The potential utility of the nanochannels in biologically relevant applications—*e.g.*, size-based separation of biomolecules—is demonstrated by imaging aggregates of amyloid beta (Aβ), the amyloidogenic peptide implicated in Alzheimer's disease (AD).[18] The size of the Aβ aggregate that can enter a nanochannel is found to be dependent on the channel cross-section.

Experimental

The general principle of fabrication is schematically outlined in Fig. 1. The nanochannels are fabricated from a heterostructure

[a]*L-NESS, Dipartimento di Fisica, Politecnico di Milano, Via Anzani 42, 22100 Como, Italy. E-mail: roman.sordan@como.polimi.it; Fax: +39 031 332 7617; Tel: +39 031 332 7622*
[b]*Dipartimento di Medicina Sperimentale, Università degli Studi di Milano-Bicocca, Via Cadore 48, 20052 Monza, Italy*
[c]*L-NESS, Dipartimento di Scienza dei Materiali, Università degli Studi di Milano-Bicocca, Via R. Cozzi 53, 20125 Milano, Italy*
[d]*Max-Planck-Institut für Festkörperforschung, Heisenbergstr. 1, 70569 Stuttgart, Germany*
[e]*Institute de Physiques des Nanostructures, Ecole Polytechnique Fédérale de Lausanne, 1015 Lausanne, Switzerland*

† Electronic supplementary information (ESI) available: Fig. S1: Cracks in the cover adjacent to the nanochannels when the cover is evaporated under an angle of incidence of 0°; Fig. S2: Formation of an open nanochannel at the opposite side of the nanochannel sealed by evaporating the cover under an angle of incidence of 45°; Fig. S3: Fluorescence image of the control sample which demonstrates that dye fills the nanochannels instead of accumulating on top of the cover at the sidewalls; and Video S4: Dynamics of the filling of the nanochannels by capillary forces. See DOI: 10.1039/b819520j

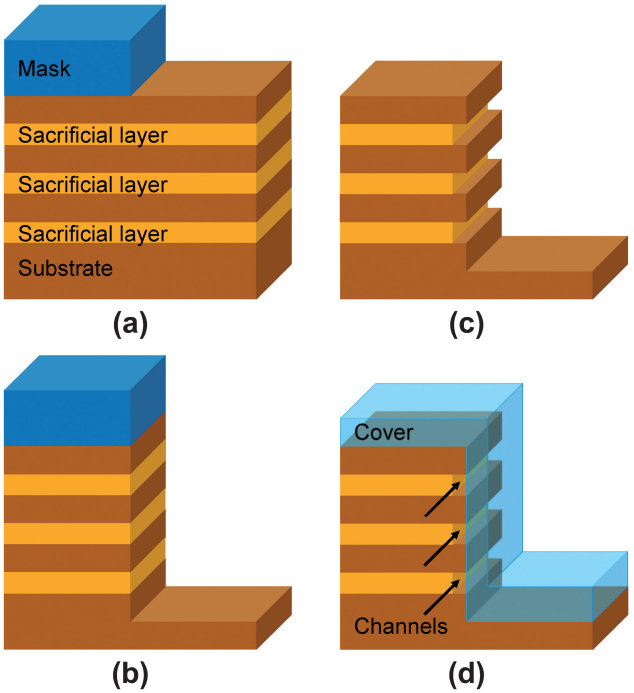

Fig. 1 Schematic showing the fabrication of a vertical array of nanochannels by side etching of thin sacrificial layers. (a) After mask deposition. (b) After etching. (c) After mask removal and selective side etching of the sacrificial layers. (d) After cover deposition. All fabrication steps can be carried out on a whole wafer.

comprised of a substrate and several thin sacrificial layers. Such a heterostructure can be made by epitaxial growth, evaporation, or spin-coating. In the first step (Fig. 1(a)), an etching mask is deposited on the top surface of the heterostructure. The mask can be mechanical or patterned by any kind of lithography since the lithographic resolution will not influence the cross-sectional size of the nanochannels. In the second step (Fig. 1(b)), the heterostructure is etched in the area not protected by the mask. Both wet (chemical) and dry (reactive ion, ion beam, *etc.*) etching can be used. The only requirement is that the heterostructure is etched deep enough to expose the lateral surface of the required number of sacrificial layers (*i.e.*, nanochannels). The sacrificial layers can also be exposed by cleaving the sample or selectively growing the heterostructure on a masked substrate. In the third step (Fig. 1(c)), the etching mask is removed and the sacrificial layers are selectively wet-etched laterally to form the nanochannels. Selectivity can also be obtained by other means, *e.g.*, by ion beam etching which can discriminate between heavier and lighter atoms or molecules. In the last step (Fig. 1(d)), the nanochannels are sealed by depositing the cover. For some applications in which the liquid is drawn into the channels by strong capillary forces, the cover may not be necessary (see Fig. 3(b)). The height of the nanochannels is determined by the thickness of the sacrificial layers, while the width is determined by the extent of side etching. Both can be easily adjusted at the nanometer scale and are independent of the feature sizes of the initial etching mask used to expose the sacrificial layers laterally (*i.e.*, independent of the resolution of the process used to create the mask). The length of the nanochannels is determined by the length of the etching mask which can in principle be a few cm.

In the present case, nanochannels were fabricated in a crystalline SiGe heterostructure epitaxially grown by low-energy plasma-enhanced chemical vapor deposition.[19] Two different substrate/sacrificial layer combinations were used: $Si_{0.3}Ge_{0.7}$/Ge ($Si_{0.3}Ge_{0.7}$ being a virtual substrate[20] grown on Si) and Si/$Si_{0.6}Ge_{0.4}$. A 100 nm thick SiO_2 cover was deposited by e-beam evaporation at an incidence angle of 45° in order to avoid the formation of a shadow mask at the step edges[21] (see Fig. S1, ESI†). At this angle, the groves are not filled by the cover.[22] For the fabrication of the nanochannels alone it is not necessary to pattern the cover. Since the nanochannels were connected to reservoirs containing liquid, the cover was patterned in order to keep the reservoirs open and channels sealed. Although the SiGe technology used does not impose any fundamental limits on the dimensions of the nanochannels, it is expected that very long nanochannels with a very small cross-section (<< 10 nm) will be clogged by the etching-induced roughness of the sidewalls. In the case of crystalline Si, this problem can be mitigated by KOH-based anisotropic etching to obtain atomically smooth surfaces of the etched sidewalls.[11]

Fig. 2(a) shows the cross-section of a sealed single-nanochannel structure fabricated by selective side etching of a 10 nm thick Ge sacrificial layer clad in $Si_{0.3}Ge_{0.7}$. The trench was created by reactive ion etching (RIE) using CF_4, while the

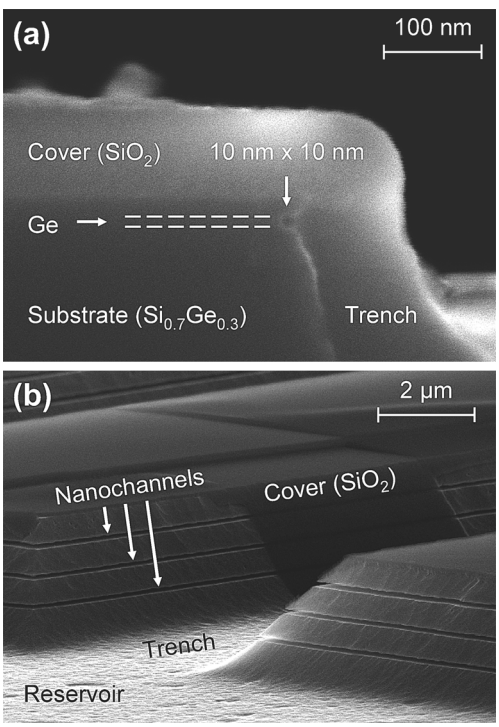

Fig. 2 Nanofluidic channels fabricated in two different types of SiGe heterostructure. (a) A single nanochannel structure obtained by a selective side etching of a Ge sacrificial layer on a $Si_{0.3}Ge_{0.7}$ virtual substrate. Prior to side etching, the nanochannel was exposed laterally by etching a trench in the substrate. The nanochannel runs perpendicular to the image and has a cross-section of 10 nm × 10 nm. (b) A structure with three nanochannels obtained by etching $Si_{0.6}Ge_{0.4}$ sacrificial layers on a Si substrate. The nanochannels have a cross-section of 130 nm × 100 nm. Vertical separation between the nanochannels is 500 nm and lateral separation is 480 nm.

nanochannel was formed by selective wet etching in a mixture of H_2O_2/H_2O at 30 °C with moderate ultrasonic agitation. Under these conditions, an etch rate of ~45 nm min^{-1} was obtained with a very good selectivity with respect to the $Si_{0.3}Ge_{0.7}$ cladding. However, nanochannels with a Ge sidewall are not very suitable for fluidic applications as a thin water-soluble GeO_2 film is formed at the Ge surface when the samples are exposed to air. More robust structures can be fabricated on Si substrates by using $Si_{0.6}Ge_{0.4}$ sacrificial layers, because both materials form a stable SiO_2 film upon exposure to air. In addition, since this material combination does not require a virtual substrate, the device can be grown faster. A three-nanochannel structure fabricated in this system is shown in Fig. 2(b). The structure was fabricated by selective side etching of 15 nm thick sacrificial layers which were grown 500 nm apart in the vertical direction. The structure was etched by RIE using SF_6/O_2, followed by a selective wet etching in a mixture of $HF/HNO_3/CH_3COOH$. Both etching processes were tuned in order to obtain oblique instead of vertical (as depicted in Fig. 1) sidewalls. Such a profile results in a spatial separation between the nanochannels which simplifies their optical characterization. The spatial separation was controlled in the range of 100 nm to 1.5 μm. Nanochannels can be made to follow corners (as shown in Fig. 2(b) and 3(b)), but if nanochannels on corners facing in different directions need to be sealed then more than one evaporation/covering step is required.

Results and discussion

The flow behavior was subsequently investigated by confocal fluorescence imaging of the nanochannels filled with fluorescent dyes. Two strategies were pursued for this purpose. In the first "static" case, the nanochannels were stained with the dye by leaving the whole sample in a solution of Sudan I dissolved in a water/dimethylsulfoxide (DMSO) mixture for a few minutes. Following this, the sample was blown dry and gently rinsed with ethanol. In this manner some dye molecules were trapped in the sealed parts of the nanochannels. Fig. 3(a) shows an overlay confocal image of the single-nanochannel structure (similar to the sample in Fig. 2(a)) using such a staining procedure. The nanochannels at the upper edge of the trenches are sealed by a 5 μm wide cover, whereas those at the lower edge are unsealed (see Fig. S2, ESI†). It is apparent from the figure that the dried dye is found only in the sealed parts of the nanochannels. Control samples were fabricated in order to exclude the possibility of dye accumulation on top of the cover at the upper trench edges (see Fig. S3, ESI†). In addition to demonstrating the capability of the liquid to enter the nanochannels, this result suggests that this method could be used as a reliable way for surface functionalization of the nanochannels. This is essential when performing biochemical reactions as the surfaces of the nanochannels are required to have a well-defined chemistry such as, for example, non-specific binding of proteins.[23]

In the second "dynamic" method, a solution of fluorescein in a water/DMSO mixture was allowed to flow through the channels and the sample was imaged at various instances of the flow. For this purpose a small drop of the dye solution was placed in the reservoir which was connected to the trenches and the nanochannels (see Fig. 2(b)). The liquid flow from the reservoir

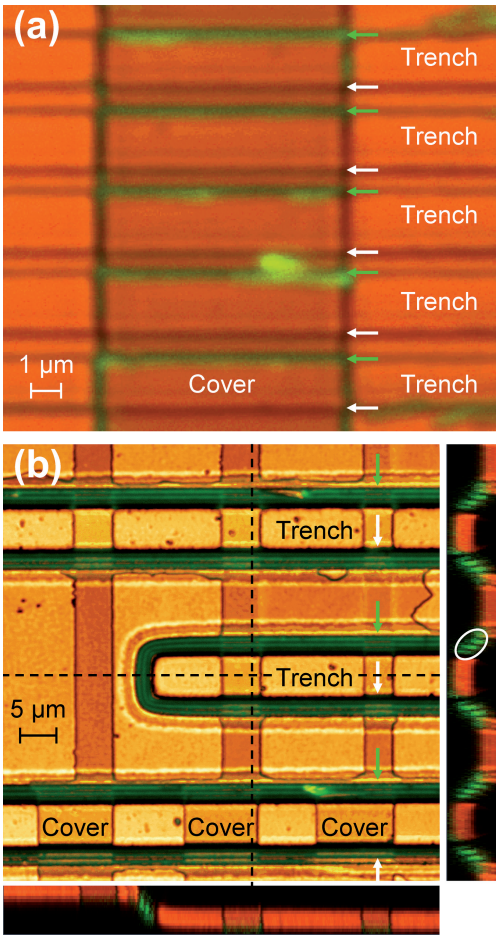

Fig. 3 Overlay (reflection and fluorescence) confocal images of the nanochannels filled with fluorescent dye. The fluorescence signal is mapped onto a green colour scale, while the reflection signal is plotted using a golden colour map. SiO_2 covers seal the nanochannels at the top edge of the trenches (marked by green arrows; white arrows mark unsealed nanochannels at the bottom edges). (a) A single nanochannel $Si_{0.3}Ge_{0.7}$/Ge structure stained with the dye Sudan I. Trench depth ~150 nm. (b) A three nanochannel $Si/Si_{0.6}Ge_{0.4}$ structure. This image was recorded at an instance when the solution containing fluorescein had filled the nanochannels. Trench depth ~2 μm. The image is an average of data collected from different confocal planes. The vertical section profiles along the dashed lines are plotted on the right and at the bottom. The topography of the sample (red/yellow signal in the profiles) and the 3 nanochannels filled with the dye solution (green signal) can be clearly visualized from these profiles (one set of the nanochannels is encircled in the section profile on the right).

into the trenches (which would themselves act as microfluidic channels) is prevented by selectively increasing the hydrophilicity of the nanochannels with respect to the trenches. This was achieved by protecting the trenches with a resist mask and subjecting the sample to oxygen plasma (1 Torr, 100 W nominal, 30 s). Subsequently, the mask was stripped off before filling the reservoir with the dye. The changes in channel surface properties rendered by this method were sufficient enough to pull the liquid into the nanochannels faster than into the trench merely by capillary forces.[24–26] Fig. 3(b) shows an overlay 3D average confocal image taken at an instance when the dye solution has filled the nanochannels from the reservoir. The dye solution is

confined within the nanochannels by strong capillary forces rendering both sealed and open parts of all three nanochannels clearly visible in the fluorescence image. The ability to distinguish the three vertical channels during imaging is possible due to a large spatial separation between the nanochannels (~1 μm) in this sample. The presence of the three channels is also apparent from the section profiles shown adjacent to the confocal image, where a fluorescence signal is clearly seen to originate almost exclusively from the three channels. The measured spatial and vertical separation obtained from such section profiles was identical to the separation measured by the scanning electron microscope.

The dynamics of the filling of the nanochannels by capillary forces can be followed by real-time confocal fluorescence images of the samples, as the dye solution spreads from the reservoirs to the nanochannels and finally to the trenches. Fig. 4 shows frames taken from a real-time video (see Video S4, ESI†) during the filling of a two-nanochannel structure. The dye solution is spreading through the sample from the top of the image towards the bottom of the image. As shown by the horizontal arrows, the liquid starts filling the open part of the lower nanochannel first followed by the upper nanochannel. The closed parts of the nanochannels (marked by the vertical arrows) are subsequently filled. Large spatial separation (~500 nm) between the nanochannels allows the individual channels to be easily identified after both of them are filled with the dye. Finally the liquid fills up the trenches. It is apparent from the figure and the video that the capillary forces in the nanochannels (even below the cover) are strong enough to pull the liquid into the nanochannels before it is pulled into the microfluidic trenches. This suggests that selective surface modification is the key to optimizing the flow behavior for the required application. Furthermore, the filling behavior of the nanochannels varies from one sample to another. This can be attributed to channel inhomogeneities which occur due to slightly different etching conditions. Nevertheless, the fabrication procedure along with the dynamic confocal measurement technique provides us with a platform that would enable the study of the behavior of tagged (bio)molecules and the progress of (bio)chemical reactions in a very confined environment such as a nanochannel.

The feasibility of using nanochannel arrays for one such biologically relevant application is demonstrated here. Monomeric Aβ peptide, released in aberrant amounts in AD, has a strong propensity to aggregate, progressively forming oligomeric, multimeric, proto-fibrillar and fibrillar aggregates, and ending with deposition of plaques, a hallmark of the disease in the brains of AD patients.[18] Among the emerging and potential therapies for AD is the treatment with drugs interfering with aggregation of Aβ, particularly into oligomers or polymers that are correlated with cellular toxicity.[27] In order to evaluate the efficacy of candidate anti-amyloidogenic drugs *in vitro*, the distribution of the various aggregation forms of the Aβ must be monitored before and after interaction with the drug. Hence, the ability to separate different forms of Aβ or to maintain them in a fixed state without further aggregation is vital for studying the effect of candidate drugs.

Fig. 5(a) shows an overlay confocal image of the reservoir in which a mixture of different aggregation forms of Aβ, labelled with the fluorescent dye diethylaminocoumarin, were deposited

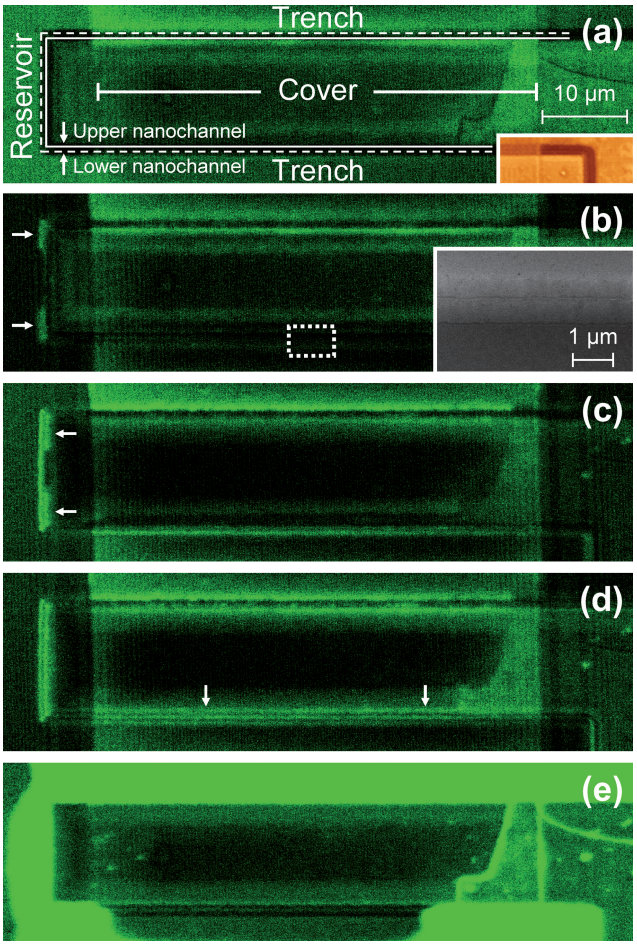

Fig. 4 Frames taken from a real-time video (captured by a confocal microscope at the rate of 1 frame s^{-1}) showing the dynamics of filling in a two-nanochannel $Si/Si_{0.6}Ge_{0.4}$ structure. A small drop of the fluorescent dye is placed in the reservoir at the start of the measurements ($t = 0$ s). The dye solution spreads from the top to the bottom of the image (a) $t = 0$ s. At the beginning, the nanochannels are empty. The upper (lower) nanochannel is outlined by a solid (dashed) line. Inset: corresponding part of the reflection image in which the empty nanochannels can be seen. (b) $t = 5$ s. The dye starts to fill the open lower nanochannel (marked by arrows). Inset: Magnified part of the marked location (dashed rectangle) showing both nanochannels. (c) $t = 11$ s. The lower channel is filled and the upper nanochannel starts to fill (marked by arrows). (d) $t = 16$ s. The open channels as well as the closed ones (below the cover indicated by arrows) are filled and can be clearly resolved. (e) $t = 63$ s. The dye solution fills up the trench and the nanochannels can no longer be resolved in some areas.

from a DMSO solution. In order to assess the capability of size selection, the same solution was let to flow through an array of nanochannels, each of them with a slightly different cross-sectional size. Fig. 5(b) shows an overlay confocal image of nanochannels in which labelled Aβ aggregates were detected. It is apparent that small aggregates are found in the smaller nanochannel, while both small and large aggregates are present in the larger nanochannel. In addition to showing that the nanochannels restrict the entry of biomolecules according to size, these images gives us an indication that the aggregation state of Aβ might be preserved inside the nanochannels. This suggests that the nanochannels could serve as building blocks of more

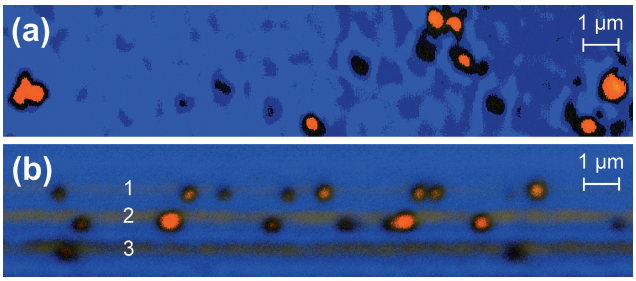

Fig. 5 Overlay (reflection and fluorescence) confocal images of labelled Aβ aggregates (a) in the reservoir and (b) in the nanochannels. The chip consists of 3 nanochannels. The smaller nanochannel (marked by 1) has a cross-section of 260 nm × 300 nm. The larger nanochannel (marked by 2) has a cross section of 310 nm × 300. The mostly empty nanochannel (marked by 3) has a cross section of 350 nm × 300 nm. Large aggregates are found only in the nanochannel 2, while small aggregates are visible both in nanochannels 1 and 2.

complex lab-on-a-chip platforms for fast screening of candidate anti-amyloidogenic drugs.

Conclusions

We have reported for the first time a simple method for the fabrication of vertical arrays of sealed nanochannels, whose cross-sectional dimensions are tunable down to 10 nm. The flow through the nanochannels was programmed by appropriate surface functionalization strategies. The capillary filling of the nanochannels with fluorescent dye solutions was tracked using a confocal laser scanning microscope. The feasibility of the use of nanochannel arrays for biological applications was demonstrated by imaging Aβ aggregates in the nanochannels. Aβ aggregates entering a nanochannel were found to be restricted according to their size. In this manner, the nanochannels could serve as an ideal platform for studying Aβ in different aggregation states, and therefore have important implications for the therapy and diagnosis of AD and of other amyloidoses.

Unlike the case of microfluidics, where microchannels have been demonstrated in 3D, work on nanofluidics is still in its infancy. Our ability to stack nanochannels one on top of another is highly promising for the subsequent realization of 3D nanofluidic circuits analogous to multi-layer electronic circuits. Lab-on-a-chip systems realized by integrating actuators with these 3D nanochannels circuits are expected to open new vistas both for high throughput biological applications as well as for fundamental studies.

Acknowledgements

This work was supported by the Cariplo foundation through the project NANODEV.

References

1 J. C. T. Eijkel and A. van den Berg, *Microfluid. Nanofluid.*, 2005, **1**, 249.
2 J. L. Perry and S. G. Kandlikar, *Microfluid. Nanofluid.*, 2006, **2**, 185.
3 D. R. Reyes, D. Iossifidis, P.-A. Auroux and A. Manz, *Anal. Chem.*, 2002, **74**, 2623.
4 D. J. Beebe, G. A. Mensing and G. M. Walker, *Annu. Rev. Biomed. Eng.*, 2002, **4**, 261.
5 M. Zwolak and M. D. Ventrax, *Rev. Mod. Phys.*, 2008, **80**, 141.
6 R. B. Schoch, J. Han and P. Renaud, *Rev. Mod. Phys.*, 2008, **80**, 839.
7 Y.-K. Choi, T.-J. King and C. Hu, *IEEE Trans. Electron Devices*, 2002, **49**, 436.
8 N. R. Tas, J. W. Berenschot, P. Mela, H. V. Jansen, M. Elwenspoek and A. van den Berg, *Nano Lett.*, 2002, **2**, 1031.
9 C. Lee, E.-H. Yang, N. V. Myung and T. George, *Nano Lett.*, 2003, **3**, 1339.
10 Y. H. Cho, S. W. Lee, B. J. Kim and T. Fuji, *Nanotechnology*, 2007, **18**, 465303.
11 X. Liang, K. J. Morton, R. H. Austin and S. Y. Chou, *Nano Lett.*, 2007, **7**, 3774.
12 X. Liang and S. Y. Chou, *Nano Lett.*, 2008, **8**, 1472.
13 R. Krahne, A. Yacoby, H. Shtrikman, I. Bar-Joseph, T. Dadosh and J. Sperling, *Appl. Phys. Lett.*, 2002, **81**, 730.
14 Y. Mei, D. J. Thurmer, F. Cavallo, S. Kiravittaya and O. G. Schmidt, *Adv. Mater.*, 2007, **19**, 2124.
15 M.-S. Chun, M. S. Shim and N. W. Choi, *Lab Chip*, 2006, **6**, 302.
16 Z. Wang, M.-C. Kim, M. Marquez and T. Thorsen, *Lab Chip*, 2007, **7**, 740.
17 J. Han and H. G. Craighead, *Science*, 2000, **288**, 1026.
18 J. Hardy and D. J. Selkoe, *Science*, 2002, **297**, 353.
19 B. Rössner, D. Chrastina, G. Isella and H. von Känel, *Appl. Phys. Lett.*, 2004, **84**, 3058.
20 C. Rosenblad, H. von Känel, M. Kummer, A. Dommann and E. Müller, *Appl. Phys. Lett.*, 2000, **76**, 427.
21 A.-L. Barabási and H. E. Stanley, in *Fractal Concepts in Surface Growth*, Cambridge University Press, 1995.
22 Directionality of the e-beam evaporation prevents complete filling of the groves unless the cover is evaporated under an angle of incidence of 90°. For other angles α, the evaporation reduces the cross sectional area of the nanochannels by a multiplying factor $1–x/2$, for $x < 1$, and $1/(2x)$, for $x > 1$, where x is $\tan(\alpha)$ divided by the aspect ratio of the groves.
23 J. Bluemmel, N. Perschmann, D. Aydin, J. Drinjakovic, T. Surrey, M. Lopez-Garcia, H. Kessler and J. P. Spatz, *Biomater.*, 2007, **28**, 4739.
24 N. Tas, J. Haneveld, H. Jansen, M. Elwenspoek and A. van den Berg, *Appl. Phys. Lett.*, 2004, **85**, 3274.
25 A. Han, G. Mondin, N. G. Hegelbach, N. F. de Rooij and U. Staufer, *J. Coll. Interf. Sci.*, 2006, **293**, 151.
26 H. E. Jeong, P. Kim, M. K. Kwak, C. H. Seo and K. Y. Suh, *Small*, 2007, **3**, 778.
27 W. J. Lukiw, *Expert Opin. Emerg. Drugs*, 2008, **13**, 255.